PHYSICAL REVIEW B **88**, 054515 (2013)

Interactions and superconductivity in heavily doped MoS_2

R. Roldán,[1] E. Cappelluti,[1,2] and F. Guinea[1]
[1]*Instituto de Ciencia de Materiales de Madrid, CSIC, Sor Juana Inés de la Cruz 3, 28049 Madrid, Spain*
[2]*Istituto dei Sistemi Complessi, U.O.S. Sapienza, CNR, via dei Taurini 19, 00185 Roma, Italy*
(Received 21 January 2013; revised manuscript received 11 August 2013; published 27 August 2013)

We analyze the microscopic origin and the physical properties of the superconducting phase recently observed in MoS_2. We show how the combination of the valley structure of the conduction band, the density dependence of the screening of the long-range Coulomb interactions, the short-range electronic repulsion, and the relative weakness of the electron-phonon interactions makes possible the existence of a phase where the superconducting order parameter has opposite signs in different valleys, resembling the superconductivity found in the pnictides and cuprates.

DOI: 10.1103/PhysRevB.88.054515 PACS number(s): 74.20.Mn, 74.25.Kc, 74.62.Dh, 74.70.−b

I. INTRODUCTION

Molybdenum disulfide (MoS_2) is a layered semiconductor which can be exfoliated down to monolayer unit cells,[1] like graphene.[2–4] The existence of an energy gap makes MoS_2 a convenient material for nanoelectronics.[5,6] Metallic behavior can be induced, also as in graphene, by means of electric field effects or by doping, and the corresponding Fermi surface is typically made up of inequivalent Fermi pockets,[7–12] defining a valley degree of freedom which is strongly entangled with the spin degree of freedom,[13] and it can be further controlled and manipulated, opening promising perspectives for spintronics. At high carrier concentrations ($n \sim 10^{14}$ cm^{-2}), and in the presence of high-κ dielectrics, MoS_2 has also been shown to undergo a superconducting transition, with a doping-dependent critical temperature $T_c(n)$ which exhibits a maximum as a function of n and drops to zero at sufficiently large values of n.[14,15]

A ferromagnetic behavior has also been reported in MoS_2,[16–19] and it has been related to edges or to the existence of defects.[20,21] The magnetic properties of MoS_2 nanoribbons indicate that the electron-electron interactions are non-negligible. The combination of significant electron-electron interactions and a two-dimensional Fermi surface made up of many pockets is also a hallmark of the cuprate and pnictide superconductors,[22] where the superconducting gap has a d-wave symmetry (cuprates) or opposite sign in different pieces of the Fermi surfaces (pnictides).[22] A related gap structure has also been proposed for heavily doped graphene when the electron-electron interaction is sufficiently large.[23]

In the present work we study the origin of superconductivity in heavily doped MoS_2, by considering the role of both electron-electron and electron-phonon interactions. We analyze first the general features of the effective interaction between charge carriers, and we make semiquantitative estimates of the strength of the different contributions to the effective coupling. We discuss next the competition between the electron-electron and electron-phonon interactions, and the possible types of superconductivity that emerge. Although a quantitative determination of the superconducting T_c is outside the scope of our work, the present analysis suggests that superconductivity in MoS_2, under the experimental conditions of Refs. 14 and 15, is likely to be induced by the electron-electron interaction, and that a superconducting phase with a nontrivial gap structure is possible.

II. EFFECTIVE INTERACTIONS

Following the experimental results of Refs. 14 and 15, we assume that the carriers leading to the superconducting phase are electronlike, confined in the first MoS_2 layer closer to the high-dielectric gate. The validity of this approximation will be discussed later. We also assume that, as in monolayer MoS_2, the electronlike carriers are located in the two inequivalent Fermi pockets centered at the K and K' corners of the Brillouin zone (see Fig. 1), having thus a sizable d-orbital character with main $d_{3z^2-r^2}$ orbital component. At sufficiently large concentrations six additional inequivalent Q valleys start to be filled, located halfway between the Γ and K points, with primary $d_{x^2-y^2}$ and d_{xy} Mo orbital character. These secondary valleys at higher charge density do not play a relevant role in our main discussion and will therefore be neglected. Their possible effect will, however, be addressed in the final discussion.

We explore here the possibility that superconductivity is induced by effective electron-electron interactions, associated with the direct Coulomb interaction between charge carriers or with the effective coupling induced by phonons. As in Ref. 23, we consider superconducting phases where the two carriers in a Cooper pair are in valleys K and K', related by time-reversal symmetry $(\mathbf{k},-\mathbf{k})$. We can now classify, as sketched in Fig. 1, the interactions leading to scattering of the Cooper pairs into intra- and intervalley couplings, namely, $V_{\text{intra}}(\vec{\mathbf{q}},\omega)$, $V_{\text{inter}}(\vec{\mathbf{q}},\omega)$, where $\vec{\mathbf{q}}$ and ω are the exchanged momentum and frequency. We consider only scattering processes of carriers near the Fermi surfaces, which are assumed to be isotropic and centered at K and K'.

The classification of the interaction into an intravalley and an intervalley component allows us to define the dimensionless coupling constants[23]

$$\lambda_\alpha = \rho(\epsilon_F)\int_0^\pi d\theta\, V_\alpha\left[2k_F \sin\left(\frac{\theta}{2}\right)\right], \qquad (1)$$

where α labels the intra- and inter valley scattering, and $\rho(\epsilon_F) = m_{\text{eff}}/(2\pi\hbar^2)$ is the density of states at the Fermi level per valley and per spin in terms of the effective mass m_{eff}. Typical values are $m_{\text{eff}} \approx 0.5m_0$,[24,25] where m_0 is the free-electron

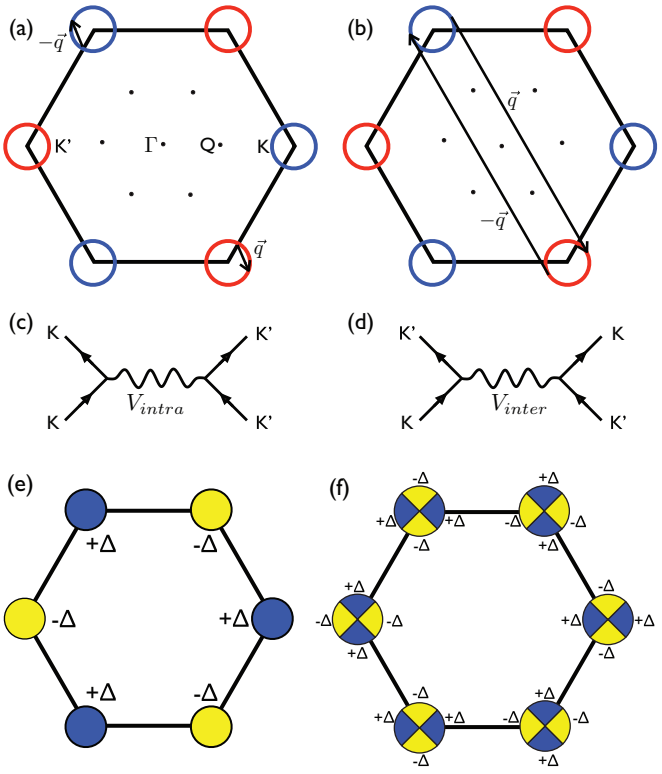

FIG. 1. (Color online) Sketch of the intravalley (a) and intervalley (b) scattering processes between Cooper pairs in MoS_2. (c) and (d) Corresponding Feynman diagrams associated with intra- and intervalley scattering. Full arrows are electron propagators, and wavy lines are effective interactions. The possible unconventional superconducting phases discussed in the text are sketched in (e) and (f).

mass. For realistic charge concentrations the Fermi wave vector is much smaller than the dimensions of the Brillouin zone, $k_F \ll |\vec{\mathbf{K}}|$, so that we can in good approximation neglect the momentum dependence of $V_{\text{intra}}(\vec{\mathbf{q}})$ and $V_{\text{inter}}(\vec{\mathbf{q}})$, except for electron-electron intravalley scattering, as discussed below.

We further neglect the dependence on frequency of the effective interactions in Eq. (1). MoS_2 has two-dimensional parabolic bands with a finite density of states, and a finite static Thomas-Fermi screening, for all carrier densities. The frequency dependence of the interactions is described by a scale comparable to ϵ_F (for the electron-electron interaction), or to ω_{ph} (for the electron-phonon interaction), where ω_{ph} is the phonon frequency. The neglect of the frequency dependence of the interaction is justified when the calculated gap is much lower than these frequencies. This constraint imposes a limit on our results, which are rigorously valid only at the onset of superconductivity. Note that the inclusion of retardation effects in the electron-electron interaction typically favors superconductivity (see Refs. 26 and 27 for a related calculation of excitonic condensation).

The existence of superconductivity requires $\lambda_{\text{intra}} \pm \lambda_{\text{inter}} < 0$, where the choice of the sign depends on whether the gaps in the two valleys have equal or opposite signs. The electron-phonon coupling leads to attractive interactions, $\lambda^{e\text{-ph}} < 0$, while the electron-electron couplings lead to repulsive interactions, $\lambda^{e\text{-}e} > 0$. However, repulsive interactions can also lead to superconductivity provided that $\lambda_{\text{inter}} > \lambda_{\text{intra}} > 0$.

A. Electron-phonon interaction

The electron-phonon interaction in single-layer MoS_2 has been evaluated in Ref. 28, finding relevant contributions from three acoustic modes and from six optical modes. Note that the coupling to the acoustic modes vanishes when the phonon wave vector approaches zero. The leading couplings identified in Ref. 28 are thus the ones to the polar LO modes, $\hbar\omega_{\text{LO}} \approx 0.048$ eV, and to the homopolar mode, $\hbar\omega_{\text{ho}} \approx 0.05$ eV, where the S atoms oscillate out of the plane.[28] The homopolar mode contributes to intravalley scattering, while the LO mode contributes to intravalley scattering, through the induced electric polarization, and also to intervalley scattering.

Using the notation in Ref. 28 we define an effective interaction, at frequencies much smaller than the phonon energies, as

$$\begin{aligned} V^{\text{LO}}_{\text{intra}} &= -\frac{g^2_{\text{LO}}}{\hbar\omega_{\text{LO}}}\Omega, \\ V^{\text{LO}}_{\text{inter}} &= -\frac{D^2_{\text{LO}}}{\hbar\omega_{\text{LO}}}\frac{\hbar}{2M\omega_{\text{LO}}}\Omega, \\ V^{\text{ho}}_{\text{inter}} &= -\frac{D^2_{\text{ho}}}{\hbar\omega_{\text{ho}}}\frac{\hbar}{2M\omega_{\text{ho}}}\Omega, \end{aligned} \tag{2}$$

where $g_{\text{LO}} \approx 0.098$ eV is the long-wavelength polar coupling, $D_{\text{LO}} \approx 2.6$ eV Å^{-1} and $D_{\text{ho}} \approx 4.1$ eV Å^{-1} are deformation potentials for the LO and homopolar modes, respectively, and Ω is the area of the unit cell. We take M for the mass of the sulfur atom, which is much lighter than Mo, and thus expected to be dominant. Adding the three contributions, we find thus:

$$\lambda^{\text{ph}}_{\text{intra}} \approx -0.36, \quad \lambda^{\text{ph}}_{\text{inter}} \approx -0.13, \tag{3}$$

which account for the respective intravalley and intervalley electron-phonon coupling constants.

B. Electron-electron interaction

After having estimated the electron-phonon coupling, we address now the electron-electron repulsive interaction. Intravalley scattering is operative only for small momenta or large distance, where, as in Ref. 23, the electron-electron interaction is determined by the screened Coulomb potential:

$$V^{e\text{-}e}_{\text{intra}}(q) = \frac{2\pi e^2}{\epsilon_0(q + q_{\text{FT}})}, \tag{4}$$

where ϵ_0 is the dielectric constant of the environment, and $q_{\text{FT}} = 2\pi e^2\rho(\epsilon_F)/\epsilon_0$ is the Thomas-Fermi wave vector.

On the other hand, the contribution of the electron-electron interaction to intervalley scattering is associated with the short-range part of the Coulomb potential. The leading term in this interaction is thus given by the Hubbard term, namely, the repulsion between two electrons with opposite spin in the same atomic orbital. Since, as we discussed above, electronic states close to the K and K' points have a dominant Mo $4d$ character, we can therefore approximate

$$V^{e-e}_{\text{inter}} \approx U_{4d}\Omega, \tag{5}$$

resulting thus in a $\mathbf{k}$-independent and density-independent interaction.

Two remarks are pertinent here. First, note that the superconductivity discussed in this work is mediated by

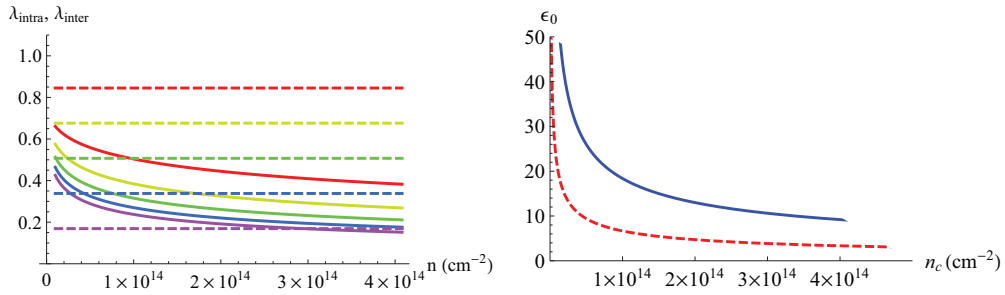

FIG. 2. (Color online) Left: Intravalley and intervalley dimensionless couplings $\lambda^{e\text{-}e}_{\text{intra}}$ and $\lambda^{e\text{-}e}_{\text{inter}}$ due to electron-electron interactions as functions of density n, for different values of ϵ_0 and U_{4d}. Full lines, λ_{intra} (from top to bottom: $\epsilon_0 = 10,20,30,40,50$); broken lines, λ_{inter} (from top to bottom: $U_{4d} = 10$, 8, 6, 4, 2 eV). Right: Relation between the critical carrier density n_c required for the existence of superconductivity and the dielectric constant of the environment, ϵ_0. Solid blue curve, $U_{4d} = 2$ eV; dashed red curve, $U_{4d} = 4$ eV.

the short-range, intervalley, electron-electron interaction. The energy scale over which this coupling acts is set by either the on-site repulsion or the electron bandwidth, whichever has the lowest value. Hence, the relevant value of the electron-electron interaction is not renormalized by screening by electron-hole pairs whose energy lies between the bandwidth and the Debye frequency as in the case of superconductivity mediated by the electron-phonon interaction.

Second, we emphasize that the long-range part of the electron-electron interaction is affected by screening processes which occur at distances from the MoS_2 layer comparable to the range of the interaction. The presence of a high-κ dielectric in the experiments analyzed here suppresses the long-range Coulomb interaction. The numerical estimates presented below suggest that the limit as $q \to 0$ of the electron-electron interaction will drop below the value of the short-range interaction, invalidating a simple extrapolation of the Hubbard model to the low-q regime.

III. RESULTS

We discuss now the consequences of the electron-phonon vs electron-electron and the intra- vs intervalley interaction in regard to the superconducting order. Along this line, unfortunately, the values of the dielectric constant ϵ_0 and of the Hubbard term U_{4d} are not well known. What it is know is that the experiments reported in Refs. 14 and 15 are done in the presence of a dielectric (HfO_2) with a high value of $\epsilon_0 \sim 25$. The ionization energies[29] of the Mo atom allow us to make an order of magnitude estimate of U_{4d}. Alternatively, we can calculate the Coulomb integral for the $4d$ orbitals of Mo, or replace the orbital by a charged sphere with the same radius. All these different approaches converge on the order of magnitude of the Hubbard repulsion, but a more accurate determination of its specific value is lacking. In this situation, we will consider U_{4d} and ϵ_0 as free-variable parameters and we will investigate their effects on the superconducting properties of MoS_2 in the ranges $\epsilon_0 \approx 10$–50 and $U_{4d} \approx 2$–10 eV.

The left panel of Fig. 2 shows the dependence of the intravalley and intervalley electron-electron coupling constants $\lambda^{e\text{-}e}_{\text{intra}}$ and $\lambda^{e\text{-}e}_{\text{inter}}$ on the specific values of ϵ_0 and U_{4d}. In particular, the intravalley coupling $\lambda^{e\text{-}e}_{\text{intra}}$ shows an initial significant dependence on density, due to the screening increase with density for $q_{\text{FT}} \lesssim k_F$, whereas $\lambda^{e\text{-}e}_{\text{intra}}$ saturates for $q_{\text{TF}} \gg k_F$. A comparison with the corresponding coupling constants for electron-phonon interaction, provided by Eq. (3), shows that the values of $\lambda^{e\text{-}e}_{\text{intra}}$ and $\lambda^{e\text{-}e}_{\text{inter}}$ in the limit of high dielectric constant (as it is the case for the experiments of Refs. 14 and 15 and moderate U_{4d} are larger in this regime than those of $\lambda^{e\text{-ph}}_{\text{intra}}$ and $\lambda^{e\text{-ph}}_{\text{inter}}$, suggesting thus that superconductivity is due to the electron-electron interaction. Furthermore, since $\lambda_{\text{inter}} = \lambda^{e\text{-ph}}_{\text{inter}} + \lambda^{e\text{-}e}_{\text{inter}} > 0$, the superconducting phase is expected to have gaps with opposite signs in the two valleys, as sketched in Fig. 1(e). Note that superconductivity of this type is possible only when the carrier density n satisfies the condition $\lambda_{\text{intra}}(n) - \lambda_{\text{inter}} < 0$. This inequality defines a critical density n_c above which superconductivity appears. The dependence of n_c on the dielectric constant of the environment is shown in the right panel of Fig. 2.

Apart from the more likely symmetry of the gap discussed above, it is worth noticing that an additional superconducting phase is possible because of the modulation of the electron-electron interaction due to screening. This mechanism always leads to an order parameter with a modulated k-dependent gap within each valley[30] [see Fig. 1(f)]. However, the resulting critical temperatures for this phase are typically very low,[23] so that it is very unlikely to be related to the experimental evidence of superconductivity in MoS_2.

IV. SUPERCONDUCTING PHASE AND OPEN QUESTIONS

The change in sign of the superconducting gap in the two valleys implies that the superconducting phase in MoS_2 has unusual properties with respect to conventional superconductors. More specifically we can recall the following:[30] (i) Elastic scattering is pair breaking, leading to the suppression of superconductivity when $v_F/\ell \gtrsim |\Delta|$, where $v_F = \hbar k_F/m_{\text{eff}}$ is the Fermi velocity, ℓ is the elastic mean free path, and Δ is the superconducting gap; (ii) strong scatterers induce localized Andreev states within the gap; (iii) Andreev states also appear at certain edges. However, unlike graphene, it should be recalled that MoS_2 also shows a significant spin-orbit coupling, so that the combination of a nontrivial superconducting order parameter with the spin-orbit coupling can lead to other interesting properties.

An intriguing role in the above scenario is played by the specific value of the effective mass m_{eff}. Apart from the determination of the effective couplings, this parameter

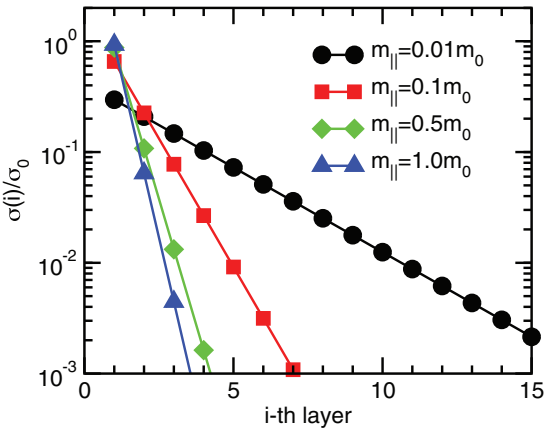

FIG. 3. (Color online) Distribution of the electric charge per layer $n(i)$ in multilayer MoS_2 under gated conditions for $n = 10^{14}$ cm^{-2}, for different values of the effective mass.

is relevant in assessing the robustness of the Fermi surface structure depicted in Fig. 1. The previous analysis was based on the assumption of an electronic structure similar to that in monolayer MoS_2, where the carriers occupy two inequivalent valleys corresponding to the absolute minima in the conduction band at the K and K' points. However, it should be recalled that six inequivalent secondary minima are also predicted at the Q points, midway between the Γ and the K and K' points, shown by the dots in Fig. 1. In bilayer and multilayer MoS_2 the minima at the Q points are expected to lie below the valleys at the K and K' points, and in monolayer MoS_2 the minima in Q start to be filled at sufficiently high carrier densities, once the pockets in K and K' are partially filled. Since the relative filling of the pockets at the K and K' and the Q points depends on the corresponding effective masses, an accurate determination of $m_{\rm eff}$ could also assess the possible presence of Fermi pockets at the Q points. It should be noted also that the value of the effective mass $m_{\rm eff}$ determines the screening properties and, as a result, the distribution of the gate-induced charge in the multilayer MoS_2. In Ref. 15 it was suggested that, because of the strong electric field, carriers are mainly localized in the first layer close to the high-dielectric gate (note that the high carrier densities enhance the screening and thus the confinement).

Theoretical first-principles-based calculations indicate a mass $m_{\rm eff}$ of the order $m_{\rm eff} \approx 0.4\, m_0$–$1m_0$,[7–11,24,25,31] whereas early experimental measurements suggest $m_{\rm eff}$ ranging from $\sim 0.01m_0$ (Ref. 32) to $\sim 1m_0$.[33–35] In the absence of a definitive estimate of $m_{\rm eff}$, we checked the dependence of the induced charge distribution on $m_{\rm eff}$ by performing a Thomas-Fermi-like calculation using a similar model for the screening of a MoS_2 multilayer as in Ref. 36. The results for the densities achieved in the experiments $n \approx 10^{14}$ cm^{-2},[15] using different possible values of $m_{\rm eff}$, are shown in Fig. 3. They confirm that for $m_{\rm eff} \gtrsim 0.1m_0$ the charge is indeed confined only in the layer closest to the high-κ gate.[15] Note that, since the charge is strongly concentrated in the first layer, an appropriate generalization of the model on a discrete layer distribution was here employed, whereas the original continuum model of Ref. 36 would be inappropriate. Our results corroborate thus the initial assumption that the single-layer model is valid and only the K and K' valleys are occupied for the densities that lead to superconductivity in.[14,15]

It is worth mentioning, however, that exotic superconducting phases, with a gap with different signs in different valleys as sketched in Fig. 1(e), are expected to appear also in the cases when only the Fermi pockets at the Q points are filled (expected in the low-density regime when the carriers are spread among a few layers) or even in the case at higher fillings where both pockets (Q and K) are occupied. Such exotic phases would share a similar phenomenology as in the case here considered of only two valleys at the K and K' points, in particular in regard to the features (i)–(iii) mentioned above.

As final consideration, it should be remarked that our analysis implies that the main dependence of the superconducting phase on the charge density is by the suppression of the long-range Coulomb repulsion, due to the higher screening at higher charge concentrations (see Fig. 2). Hence, our analysis at this level does not account for the decrease of T_c observed at high carrier densities $n \gtrsim 1.3 \times 10^{14}$ cm^{-2}.[15] A possible explanation for this behavior could be the change in the orbital character of the states close to the K and K' points, which lose $4d$ orbital character at higher doping, resulting in a weaker Hubbard-like intervalley interaction, or the change in the topology of the Fermi surface, as the Q valleys start to be filled.

V. CONCLUSIONS

In this paper we have analyzed the appearing of a superconducting phase of MoS_2 at high carrier concentrations and for strong screening of the long-range Coulomb potential, which is the regime experimentally relevant.[14,15] The significant short-range repulsion between carriers at the conduction band allows for a superconducting phase induced by the electron-electron interaction, where the gap acquires opposite signs in the two inequivalent pockets of the conduction band. This superconducting state, similar to that found in the cuprate and pnictide superconductors, is expected to show interesting topological features, such as Andreev states at edges and grain boundaries.

ACKNOWLEDGMENTS

F.G. acknowledges financial support from MINECO, Spain, through Grant No. FIS2011-23713, and the European Union, through Grant No. 290846. R.R. acknowledges financial support from the Juan de la Cierva Program (MINECO, Spain). E.C. acknowledges the Marie Curie Grant No. PIEF-GA-2009-251904.

[1] Q. Wang, K. Kalantar-Zadeh, A. Kis, J. Coleman, and M. Strano, Nat. Nanotechnol. **7**, 699 (2012).

[2] K. S. Novoselov, D. Jiang, F. Schedin, T. J. Booth, V. V. Khotkevich, S. V. Morozov, and A. K. Geim, Proc. Natl. Acad. Sci. USA **102**, 10451 (2005).

[3] K. S. Novoselov, A. K. Geim, S. V. Morozov, D. Jiang, M. I. Katsnelson, I. V. Grigorieva, S. V. Dubonos, and A. A. Firsov, Nature (London) **438**, 197 (2005).

[4] K. F. Mak, C. Lee, J. Hone, J. Shan, and T. F. Heinz, Phys. Rev. Lett. **105**, 136805 (2010).

[5]B. Radisavljevic, A. Radenovic, J. Brivio, V. Giacometti, and A. Kis, Nat. Nanotechnol. **6**, 147 (2011).
[6]Y. Zhang, J. Ye, Y. Matsuhashi, and Y. Iwasa, Nano Lett. **12**, 1136 (2012).
[7]R. V. Kasowski, Phys. Rev. Lett. **30**, 1175 (1973).
[8]D. W. Bullett, J. Phys. C **11**, 4501 (1978).
[9]R. Coehoorn, C. Haas, J. Dijkstra, C. J. F. Flipse, R. A. de Groot, and A. Wold, Phys. Rev. B **35**, 6195 (1987).
[10]T. Böker, R. Severin, A. Müller, C. Janowitz, R. Manzke, D. Voß, P. Krüger, A. Mazur, and J. Pollmann, Phys. Rev. B **64**, 235305 (2001).
[11]S. Lebègue and O. Eriksson, Phys. Rev. B **79**, 115409 (2009).
[12]E. Cappelluti, R. Roldán, J. A. Silva-Guillén, P. Ordejón, and F. Guinea, Phys. Rev. B **88**, 075409 (2013).
[13]D. Xiao, G.-B. Liu, W. Feng, X. Xu, and W. Yao, Phys. Rev. Lett. **108**, 196802 (2012).
[14]K. Taniguchi, A. Matsumoto, H. Shimotani, and H. Takagi, Appl. Phys. Lett. **101**, 042603 (2012).
[15]J. T. Ye, Y. J. Zhang, R. Akashi, M. S. Bahramy, R. Arita, and Y. Iwasa, Science **338**, 1193 (2012).
[16]J. Zhang, J. M. Soon, K. P. Loh, J. Yin, J. Ding, M. B. Sullivian, and P. Wu, Nano Lett. **7**, 2370 (2007).
[17]Y. Li, Z. Zhou, S. Zhang, and Z. Chen, J. Am. Chem. Soc. **130**, 16739 (2009).
[18]S. Mathew, K. Gopinadhan, T. K. Chan, X. J. Yu, D. Zhan, L. Cao, A. Rusydi, M. B. Breese, S. Dhar, Z. X. Shen *et al.*, Appl. Phys. Lett. **101**, 102103 (2012).
[19]Y. Ma, Y. Dai, M. Guo, C. Niu, Y. Zhu, and B. Huang, ACS Nano **6**, 1695 (2012).
[20]A. Vojvodic, B. Hinnemann, and J. K. Nørskov, Phys. Rev. B **80**, 125416 (2009).
[21]C. Ataca, H. Sahin, E. Akturk, and S. Ciraci, J. Phys. Chem. C **115**, 3934 (2011).
[22]I. I. Mazin, Nature (London) **464**, 183 (2010).
[23]F. Guinea and B. Uchoa, Phys. Rev. B **86**, 134521 (2012).
[24]E. S. Kadantsev and P. Hawrylak, Solid State Commun. **152**, 909 (2012).
[25]H. Peelaers and C. G. Van de Walle, Phys. Rev. B **86**, 241401 (2012).
[26]Y. E. Lozovik, S. L. Ogarkov, and A. A. Sokolik, Philos. Trans. R. Soc., A **368**, 5417 (2010).
[27]I. Sodemann, D. A. Pesin, and A. H. MacDonald, Phys. Rev. B **85**, 195136 (2012).
[28]K. Kaasbjerg, K. S. Thygesen, and K. W. Jacobsen, Phys. Rev. B **85**, 115317 (2012).
[29]See http://www.webelements.com/molybdenum/.
[30]W. Kohn and J. M. Luttinger, Phys. Rev. Lett. **15**, 524 (1965).
[31]P. Harper, J. Phys. C **7**, 1247 (1974).
[32]B. Evans and P. Young, Proc. Phys. Soc., London **91**, 475 (1967).
[33]R. Kaplan, Phys. Rev. B **14**, 4647 (1976).
[34]B. J. Mrstik, R. Kaplan, T. L. Reinecke, M. Van Hove, and S. Y. Tong, Phys. Rev. B **15**, 897 (1977).
[35]E. Fortin and F. Raga, Phys. Rev. B **11**, 905 (1975).
[36]A. Castellanos-Gomez, E. Cappelluti, R. Roldán, N. Agraït, F. Guinea, and G. Rubio-Bollinger, Adv. Mater. **25**, 899 (2013).